

X-ray Observations of LINER and Starburst Galaxies

P. Serlemitsos, A. Ptak, and T. Yaqoob

NASA GSFC/LHEA, Code 662, Greenbelt MD 20771

Abstract. We present the results of *ASCA* observations of a heterogeneous sample of 15 spiral galaxies. 8 are LINERs or low-luminosity AGN (LLAGN), 5 are starburst galaxies and 2 are normal spiral galaxies. We find that in all cases the *ASCA* spectra can be described by a canonical model consisting of a power-law with a photon index, $\Gamma \sim 1.7 - 2.0$, plus a soft optically thin emission component with $kT \sim 0.6 - 0.8$ keV. The implied element abundances are often sub-solar. The soft component is usually extended and the nuclear, point-like emission is sometimes absorbed by column densities in the range $\sim 10^{21} - 10^{23}$ cm $^{-2}$. The relative luminosities of the soft and hard components vary from galaxy to galaxy. For the LINERs, the 2-10 keV luminosity of the hard component is typically $\sim 10^{40-41}$ ergs s $^{-1}$ whereas the 0.5-2.0 keV luminosity of the soft component is typically $\sim 10^{39-40}$ ergs s $^{-1}$. For starbursts, the 2-10 keV luminosity of is $\sim 10^{39-40}$ ergs s $^{-1}$, somewhat lower than the corresponding luminosity of most of the LINERs in our sample. The hard component is similar to the observed X-ray spectra of quasars and also to the *intrinsic* X-ray spectra of classical Seyfert galaxies. Most of the galaxies in our sample exhibit no significant ($\Delta I/I > 20\%$) short-term variability (with timescales of a day or less) whereas long-term variability is common. We present a case study of the LINER M81 in detail where there is evidence of large-amplitude ($\Delta I/I \sim 70\%$) variability over several weeks. There is also clear evidence for a broad, complex Fe-K emission line which is compatible with an origin in an accretion disk viewed at ~ 40 degrees. These results suggest a strong connection between classical AGN, LINERs, and starburst galaxies.

1. Introduction

Optical emission lines are found in the nuclei of three types of galaxies: active galactic nuclei (AGN), low-ionization emission line regions (LINERs; Heckman, 1980) and starburst galaxies. The dominant physical process driving the emission lines in AGN is thought to be accretion onto a supermassive ($M \sim 10^5-9 M_{\odot}$) black-hole, while in starbursts the lines are the result of a current or recent episode of star formation. However, the physical origin of the line emission in LINERs is still unclear (see review by A. Filippenko in this volume). The two most likely scenarios are AGN-type accretion or starburst-type activity (i.e., shocks from supernovae). X-ray observations provide important clues to distinguish between them. AGN are compact ($\ll 1$ pc), variable sources in which the

X-ray emission has a nonthermal, power-law form. In addition, Seyfert galaxies are characterized by strong Fe K line emission produced by fluorescence in cold matter. On the other hand, nuclear starbursts are frequently extended over kpc scales and are expected to have thermal spectra characterized by coronal X-ray emission lines.

Below we shall see that the *ASCA* (See Tanaka, Inoue & Holt 1994) spectra of low-luminosity spiral galaxies are complex, usually requiring a two-component description. Previous X-ray studies have been hampered by the lack of instrument sensitivity, spectral resolution and restricted energy bandpass. In particular, the *hard* X-ray spectra were studied with non-imaging instruments where confusion of more than one bright source in the galaxy was a hinderance.

The X-ray satellite *ASCA*, launched in 1993, is capable of 0.4-10 keV imaging, spectroscopy and temporal analysis. *ASCA* is the first imaging X-ray satellite sensitive above 4 keV and has better spectral resolution ($\Delta E/E \sim 2\%$ at 6 keV) than any X-ray imaging mission to date. The half-power radius of the X-ray mirrors is $\sim 1.5'$ and this is sufficient to obtain individual spectra of sources separated by $\sim 3 - 4'$ or more (typical of the bright sources found in galaxies in our sample). Here we present preliminary *ASCA* results on a sample of fifteen galaxies (some previously published), eight of which are LINERS/LLAGN. When available, some limited analysis was also performed with public *ROSAT* data.

2. Observations

A log of the *ASCA* and *ROSAT* (*PSPC* only) observations is given in Table 1. The *ASCA* data were reduced in a manner similar to the procedures described for NGC 3147 (Ptak *et al.* 1996) and NGC 3628 (Yaqoob *et al.* 1995a). Briefly, *ASCA* consists of two solid-state imaging spectrometers (SIS; hereafter S0 and S1) and two gas imaging spectrometers (GIS; hereafter G2 and G3). The spectra were typically accumulated from counts within $3'$ of the source centroid in the case of the SIS and $4'$ in the case of the GIS. In contrast to the SIS, the GIS introduces its own broadening to the PSF of the X-ray mirrors. The background was subtracted using counts in an annulus surrounding the source, typically $\sim 6' - 12'$. Larger source and background regions were used in the case of extended sources and for some sources the spectra from different CCD chips were combined. However, note that for most of the galaxies in this sample, statistical errors dominate current instrumental uncertainties.

3. Images

For most of the galaxies in our sample, the hard (i.e., $E > 2$ keV) flux is unresolved while the soft flux is extended over a region greater than $\sim 1'$ in extent (see, e.g., Makishima *et al.* 1994; Tsuru *et al.* 1994; Terashima *et al.* 1994). Most of the galaxies have multiple point sources resolved by *ROSAT* while multiple sources are resolved by *ASCA* in only about half of the galaxies in our sample (see Table 1): NGC 1313 (Petre *et al.* 1994), NGC 3628 (Yaqoob *et al.* 1995a), M33 (Takano *et al.* 1994), NGC 253, M81 (Ishisaki *et al.* 1996), and possibly NGC 4258 (Makishima *et al.* 1994). Note that the spatial resolution

Table 1. Log of *ASCA* and *ROSAT* Observations

Galaxy	Det.*	Date	Exp. (ks)	N_{H}^{\dagger}	Dist. (Mpc)	No. of Srcs.
M33	A	7/22-23/93	~ 40	6.3^b	1.2^a	1
	P	1/7-9/93	16			1
NGC 253	A	6/12-13/93	27-33	1.3^b	2.5^h	3
	P	12/25/91-6/05/92	23			5
M81	A	See §6		4.3^b	3.6^j	3
	P	4/3-24/93	19			7
M82	A	4/19-20/93	15-20	4.3^b	3.6^j	1
	P	3/28/91-10/16/91	23			1
NGC 1313	A	7/13/93	28-29	3.7^g	4.5^f	3
	P	4/24/91-5/11/91	13			8
NGC 6946	A	5/31-6/1/93	20-30	$20 - 50^{b,i}$	8.3^d	1
	P	6/16-21/92	37			9
NGC 4258	A	5/15-16/93	36	1.2^b	10.2^d	1
	P	11/11-15/93	20			3
M51	A	5/11-12/93	33-36	1.3^b	14.0^a	2
	P	11/28/91-12/13/91	22			10
NGC 3628	A	12/12/93	18-20	2.0^c	14.9^a	2
	P	11/23-26/91	14			6
NGC 3310	A	4/17/94	18-19	1.1^b	19.4^a	1
	P	11/17-18/91	9			5
NGC 3998	A	5/10-11/94	32-39	1.2^a	24.3^k	1
	P	5/22-24/91	57			1
NGC 4594	A	1/20/94	19-22	3.8^b	22.6^a	1
	P	7/15-19/92	11			3
NGC 4579	A	6/25-26/95	~ 40	1.8^e	36.1^a	1
	P	12/15-16/91	9			1
NGC 3079	A	5/09-10/93	29-38	0.8^b	28.8^a	1
	P	11/14-15/91	19			1
NGC 3147	A	9/30/93	25-35	2.5^e	56.4^a	1
	P	10/16-22/93	9			1

All distances assuming $H_0 = 50 \text{ km s}^{-1} \text{ Mpc}^{-1}$ and $q_0 = 0$.

* A = *ASCA*, P = *ROSAT PSPC* † Galactic column in units of 10^{20} cm^{-2}

^a Soifer, B. T., *et al.* 1987, ApJ, 320, 238

^b Fabbiano, G., *et al.* 1992, ApJS, 80, 531

^c Hartmann, D., & Burton, W. 1995, In The Leiden-Dwingeloo Atlas of Galactic Neutral Hydrogen (Cambridge: Cambridge University Press, UK), in press

^d Tully, R. 1988, Nearby Galaxy Catalog (Cambridge University Press)

^e Stark, A., *et al.* 1992, ApJS, 79, 77

^f de Vaucouleurs, G. 1963, ApJ, 137, 720

^g Cleary, M., *et al.* 1979, A&AS, 36, 95

^h de Vaucouleurs, G. 1978, ApJ, 224, 710 and Davidge, T. & Pritchett, C. 1990, AJ, 100, 102

ⁱ Burnstein, D. & Heiles, C. 1984, ApJS, 54, 33

^j Freedman, W., *et al.* 1994, ApJ, 427, 628

^k de Vaucouleurs, G., *et al.* 1991, Third Reference Catalogue of Bright Galaxies (New York: Springer-Verlag)

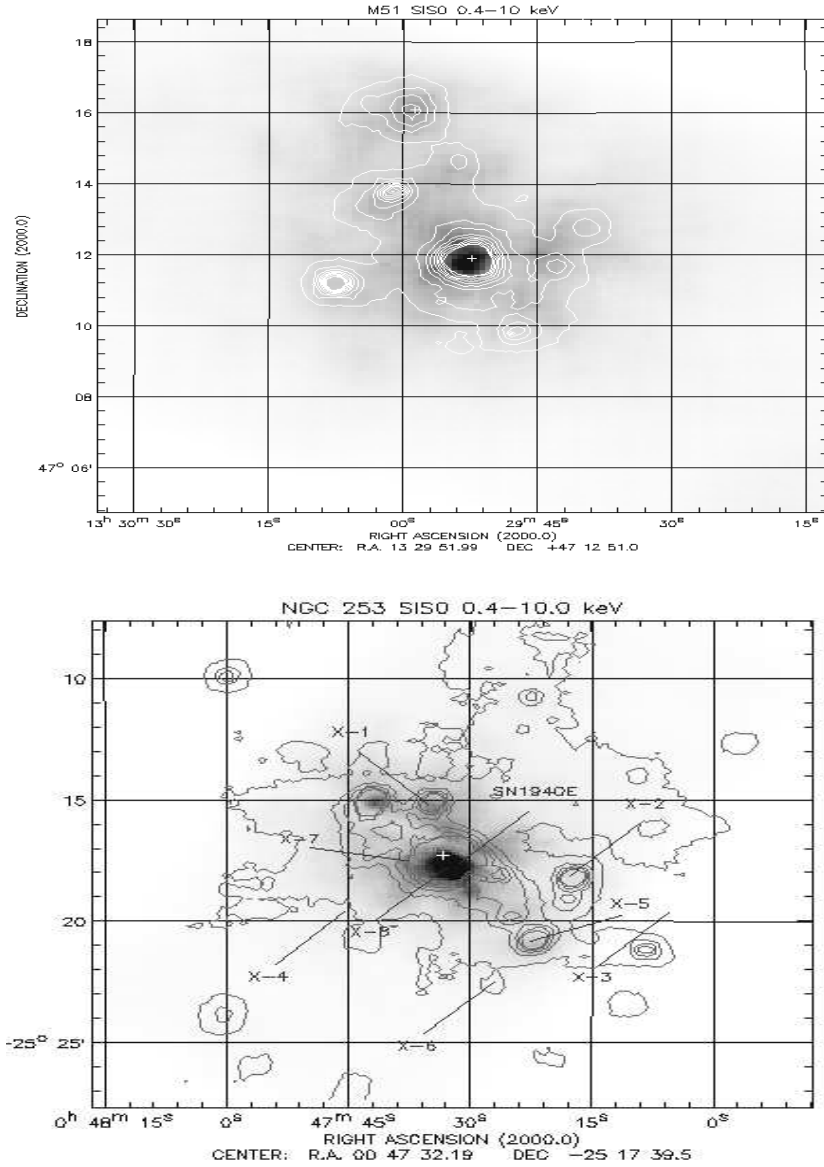


Figure 1. M51 (top) and NGC 253 (bottom) *ASCA* S0 0.4-10.0 keV images with *ROSAT* *PSPC* 0.1-2.4 keV contours, adaptively smoothed to a minimum of SNR of ~ 7 (without background subtraction). The contours are linearly spaced from 2 to 20 smoothed counts. The crosses show the locations of the optical nuclei given in NED for NGC 253, M51 (NGC 5194) and its companion (NGC 5195). Although these observations were performed in 4-CCD mode, only chips 1 and 2 have a significant number of source counts (note that the dark lanes in the S0 images are due to a gap between the chips). The M51 *ROSAT* positions were shifted as described in Marston *et al.* (1995) and the *ASCA* image was registered with the *ROSAT* image (using only 0.5-2.0 keV photons). The NGC 253 images have not been shifted. For distances of 14 Mpc (M51) and 2.5 Mpc (NGC 253), $1' = 4.0$ and 0.7 kpc, respectively.

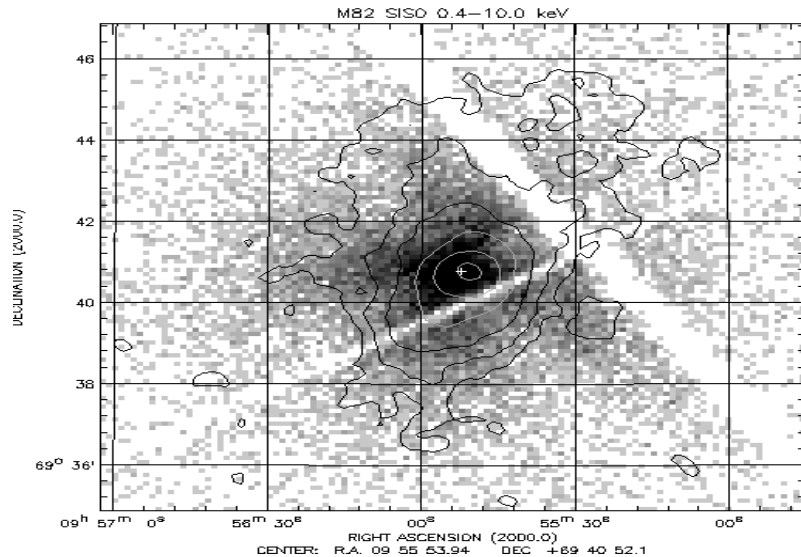


Figure 2. M82 *ASCA* S0 0.4-10.0 keV image with *ROSAT* PSPC 0.1-2.4 keV contours. The *ROSAT* image has been smoothed with a 12.5'' Gaussian and the contours are logarithmically spaced. The gaps in the S0 image are due to spacings between the CCD chips. The cross shows the location of the optical nucleus. For a distance of 3.6 Mpc, 1' = 1 kpc.

of the *ROSAT* PSPC is a factor of ~ 6 better than the *ASCA* SIS. Figures 1 and 2 show the 0.4-10.0 keV *ASCA* S0 images of M51, NGC 253, and M82, overlaid with *ROSAT* PSPC (0.1-2.4 keV) contours. Multiple sources are clearly visible in both NGC 253 and M51 (most notably M51's companion), whereas both the *ASCA* and *ROSAT* images of M82 are dominated by a nuclear source with diffuse extended emission (most visible in a NW plume spanning $\sim 5' = 5$ kpc). Some of the point sources in NGC 253 are clearly transient. In all of the galaxies, including the starbursts, the brightest source is typically the one in closest proximity to the optical nucleus.

4. Spectral Fitting: A Canonical Model

The images in Figures 1-2 suggest that the X-ray emission in this galaxy sample is complex. Indeed, while several of the galaxies are fit well by a simple power-law plus absorber model, multiple components are typically required. In general, all the *ASCA* spectra of the nuclear sources in each galaxy can be modelled adequately with a power law (with possible absorption in excess of Galactic) plus an optically thin thermal Raymond-Smith model (with absorption consistent with the Galactic value). We will refer to this as the canonical model for the X-ray spectra of the nuclear region of spiral galaxies. The power-law emission and excess absorption is generally associated with the compact nuclear source whereas the soft emission component is extended. Table 2 shows the results of spectral fitting with this canonical model. In some cases the soft component dominates the spectrum, in some the power law dominates, while in others both

Table 2. Absorbed Power-law + Raymond-Smith Fits to *ASCA* Spectra

Galaxy	Det.	$N_{\text{H,Gal}}^*$	kT (keV)	A/ A_{\odot}	$N_{\text{H,PL}}^*$	Γ	$\chi^2(\text{dof})$
M33 ^a	S0-S1	3.3				2.20	311(157)
M33 ^a	G2-G3	5.2				2.49	431(173)
M51	S0-S1	0.16 [†]	0.64 ^{+0.04} _{-0.05}	0.04 ^{+0.01} _{-0.01}	25 ⁺¹⁸ ₋₂₀	1.76 ^{+1.26} _{-0.98}	194.1(147)
M51	S0-G3	0.16 [†]	0.63 ^{+0.04} _{-0.04}	0.04 ^{+0.02} _{-0.01}	17 ⁺¹⁵ ₋₁₂	1.52 ^{+0.61} _{-0.51}	393.8(344)
M81	See §6						
M82	S0-S1	2.2	0.78	0.06	11.3	1.65	615.4(391)
M82	S0-G3	2.3 ^{+0.4} _{-0.5}	0.78 ^{+0.03} _{-0.04}	0.06 ^{+0.03} _{-0.02}	11.0 ^{+4.5} _{-4.3}	1.66 ^{+0.10} _{-0.09}	1448(1242)
N253	S0-S1	0.13 [†]	0.69 ^{+0.11} _{-0.07}	1.0 [†]	1.1 ^{+0.4} _{-0.4}	1.82 ^{+0.10} _{-0.11}	313.4(256)
N253	S0-G3	0.13 [†]	0.69 ^{+0.08} _{-0.07}	1.0 [†]	1.4 ^{+0.3} _{-0.3}	1.86 ^{+0.07} _{-0.06}	834.7 (747)
N1313 ^b	S0-S1	1.2 ^{+0.4} _{-0.4}				1.8 ^{+0.1} _{-0.1}	93(90)
N1313 ^b	G2-G3	1.2 ^{+1.0} _{-0.9}				1.8 ^{+0.1} _{-0.1}	91(98)
N3079	S0-S1	0.3 [†]	0.77 ^{+0.09} _{-0.16}	0.05 ^{+0.05} _{-0.03}	16 ⁺²⁴ ₋₁₆	1.44 ^{+0.49} _{-1.17}	178.6(184)
N3079	S0-G3	0.3 [†]	0.76 ^{+0.09} _{-0.16}	0.04 ^{+0.05} _{-0.03}	16 ⁺²⁷ ₋₁₃	1.76 ^{+1.02} _{-0.89}	358.0(371)
N3147 ^c	S0-S1	0.34 ^{+0.42} _{-0.34}				1.74 ^{+0.15} _{-0.13}	194.0(175)
N3147 ^c	S0-G3	0.35 ^{+0.35} _{-0.35}	0.65 [†]	1.0 [†]		1.76 ^{+0.10} _{-0.10}	504.6(514)
N3310	S0-S1	1.3 ^{+0.8} _{-0.7}	0.66 ^{+0.19} _{-0.43}	1.0 [†]		1.70 ^{+0.34} _{-0.23}	64.4(65)
N3310	S0-G3	1.3 ^{+0.8} _{-0.6}	0.68 ^{+0.18} _{-0.39}	1.0 [†]		1.73 ^{+0.16} _{-0.19}	143.5(141)
N3628 ^d	S0-G3	10 ⁺³ ₋₃	0.67 ^{+0.16} _{-0.33}	1.0 [†]		1.7 [†]	55.9(66)
N3998	S0-S1	1.0 ^{+0.2} _{-0.1}				1.99 ^{+0.05} _{-0.05}	393.5(378)
N3998	S0-G3	0.12 [†]	0.65 [†]	0.0	1.1 ^{+1.5} _{-0.4}	1.93 ^{+0.07} _{-0.07}	1046.1(1020)
N4258 ^e	G2-G3	0.12 [†]	0.5 ^{+0.2} _{-0.2}	1.0 [†]	150 ⁺²⁰ ₋₂₀	1.78 ^{+0.29} _{-0.29}	101(106)
N4579 ^f	S0-G3	0.34 ^{+0.05} _{-0.04}				1.87 ^{+0.09} _{-0.09}	
N4594	S0-S1	0.38 [†]	0.48 ^{+0.23} _{-0.14}	> 0.04	2.6 ^{+4.8} _{-1.6}	1.80 ^{+0.24} _{-0.19}	169.3(183)
N4594	S0-G3	0.38 [†]	0.64 ^{+0.20} _{-0.26}	> 0.05	5.5 ^{+3.1} _{-4.0}	1.96 ^{+0.21} _{-0.20}	332.4(385)
N6946	S0-G3	2.6 ^{+0.5} _{-0.5}	0.65 [†]	0.01 ^{+0.07} _{-0.01}	34 ⁺²⁴ ₋₂₀	2.92 ^{+0.89} _{-0.74}	461.3(452)
N6946	S0-G3	1.6 ^{+0.7} _{-0.9}	1.00 ^{+0.12} _{-0.18}	0.05 ^{+0.12} _{-0.04}	26 ⁺²⁹ ₋₂₆	2.00 [†]	449.4(452)

Errors not determined for parameters in poorly fitting models ($\chi_{\nu}^2 > 1.5$) or parameters that do not reduce χ^2 significantly. Empty fields indicate parameter was not included in fit. Parenthesis indicate 90% confidence intervals for 2 parameters.

* 10^{21} cm^{-2} . $N_{\text{H,PL}}$ is absorption in addition to $N_{\text{H,Gal}}$ applied to power-law.

† frozen parameter

^a Takano *et al.* (1994)

^b Source A from Petre *et al.* (1994)

^c Ptak *et al.* (1996)

^d Yaqoob *et al.* (1995a)

^e Makishima *et al.* (1994)

^f G. Reichert (private communication)

components contribute significantly to the overall spectrum. Figure 3 shows the differing relative contributions of the hard and soft spectral components in the LINERS NGC 4594, NGC 3079, and M51, which can be directly compared, in Figure 4, to the X-ray spectra of a typical Seyfert 1 (NGC 3227), a Seyfert 1.5 (NGC 4151) and a Seyfert 2 (Mkn 3) galaxy. It is interesting to note that in most cases the best-fitting temperature is consistently in the range $\sim 0.6 - 0.8$ keV (simulations show that this is not an artifact of the particular *ASCA* bandpass). The physical origin of this result is not yet satisfactorily understood (see §7). The elemental abundances are in many cases significantly sub-solar and the power-law photon index is typically $\Gamma \sim 1.7 - 2.0$. In a few sources the hard power law is absorbed by a column density greater than 10^{22} cm $^{-2}$. In the case of NGC 4258, the column density exceeds 10^{23} cm $^{-2}$ and the X-ray spectrum is indistinguishable from typical Seyfert 2 galaxies.

In some of the galaxies *ASCA* clearly resolves strong soft X-ray line emission. Figure 5 illustrates this by showing the residuals obtained from fitting M51, M82, and NGC 253 with an absorbed power-law plus a bremsstrahlung model for the soft component. The relative line strengths and energies are potentially powerful diagnostics of the elemental abundances, temperatures and/or excitation mechanisms of the emission regions. More detailed analysis will be presented in future work.

Statistically significant Fe K line emission is detected in only three galaxies: NGC 3147 (see Ptak *et al.* 1996), NGC 4258 (see Makishima *et al.* 1994) and M81 (see §6), with Fe K emission possibly detected in M51 (see Terashima *et al.* 1996). The implications of these results are discussed in §7.

The observed fluxes and luminosities for the sample derived from the fit parameters in Table 2 are shown in Table 3, except for NGC 1313, M33, and NGC 4579 where the “canonical” model has not yet been fitted to the data and the fluxes and luminosities were taken from Petre *et al.* (1994), Takano *et al.* (1994), and Reichert (private communication), respectively. For sources in which the power-law component is absorbed, the intrinsic luminosity can be estimated by multiplying the observed 2–10 keV (0.5–2 keV) luminosities by the factors 1.01 (1.34), 1.10 (5.16) and 1.88 (1168) for column densities of 10^{21} , 10^{22} and 10^{23} cm $^{-2}$ respectively (assuming $\Gamma = 2$). Also shown is the luminosity of the R-S component alone in the 0.5-2.0 keV band (excluding NGC 1313, M33, and NGC 4579).

Given the strong evidence for long-term variability (see below) in some of these galaxies, simultaneously fitting *ROSAT* and *ASCA* spectra that are not simultaneous may be misleading, particularly if the observed variability is primarily due to only one component in a multiple-component model. Accordingly, the *ROSAT* spectra were fit independently (to be discussed in future work), and Table 3 shows the 0.5-2.0 keV flux derived from the best fitting model.

5. Variability

No short-term (less than 1 day) variability has been observed in our galaxy sample (see, however, the discussion of M81 below), with upper limits of typically $\Delta I/I \sim 20\%$ over ~ 50 ks in the 0.8-10.0 keV bandpass (only the GIS data were used to search for short-term variability as they are less sensitive to pointing

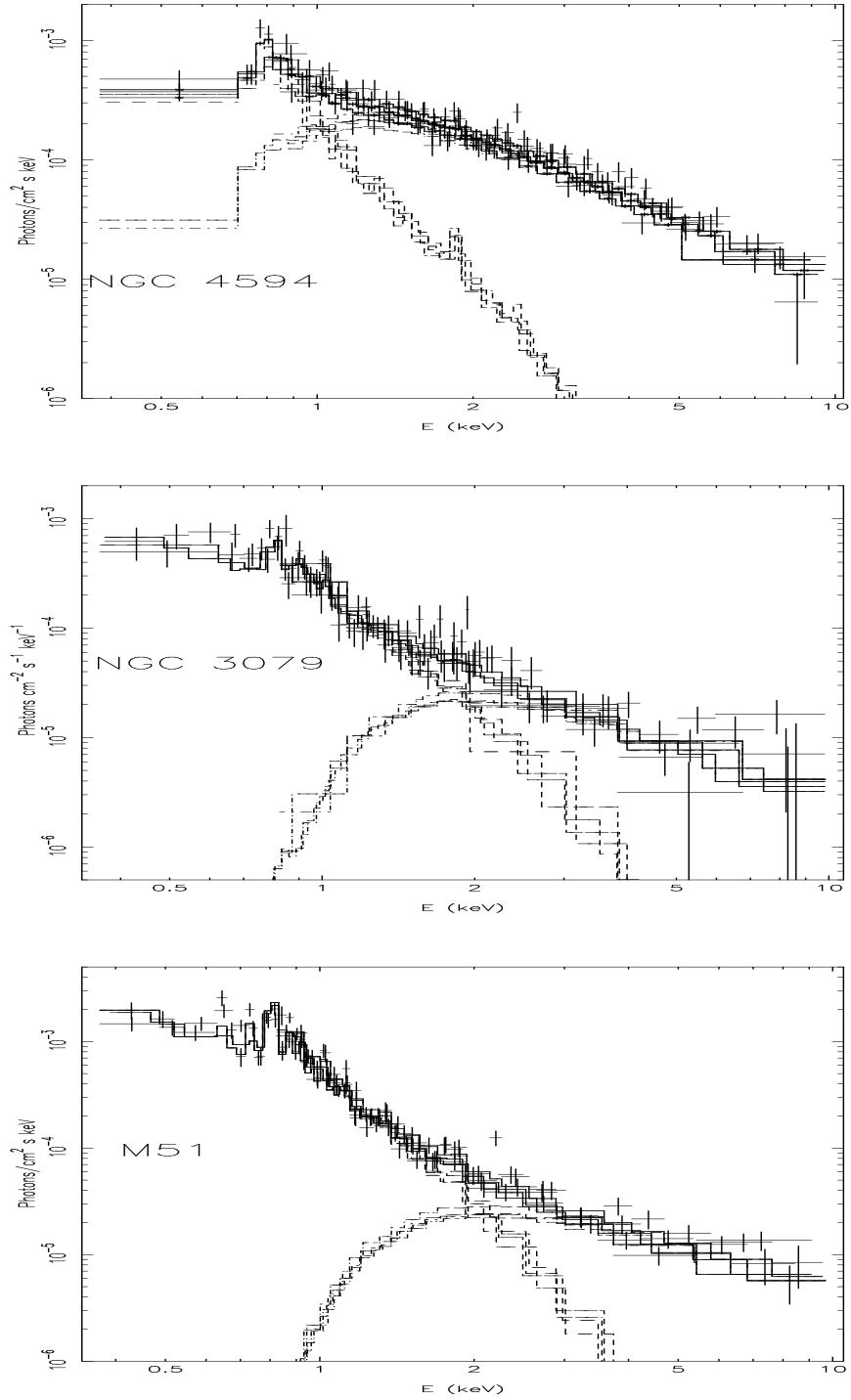


Figure 3. The unfolded *ASCA* spectra of M51, NGC 3079 and NGC 4594 (M104) when fit with the “canonical” galaxy model of an absorbed power law + coronal (Raymond-Smith) plasma.

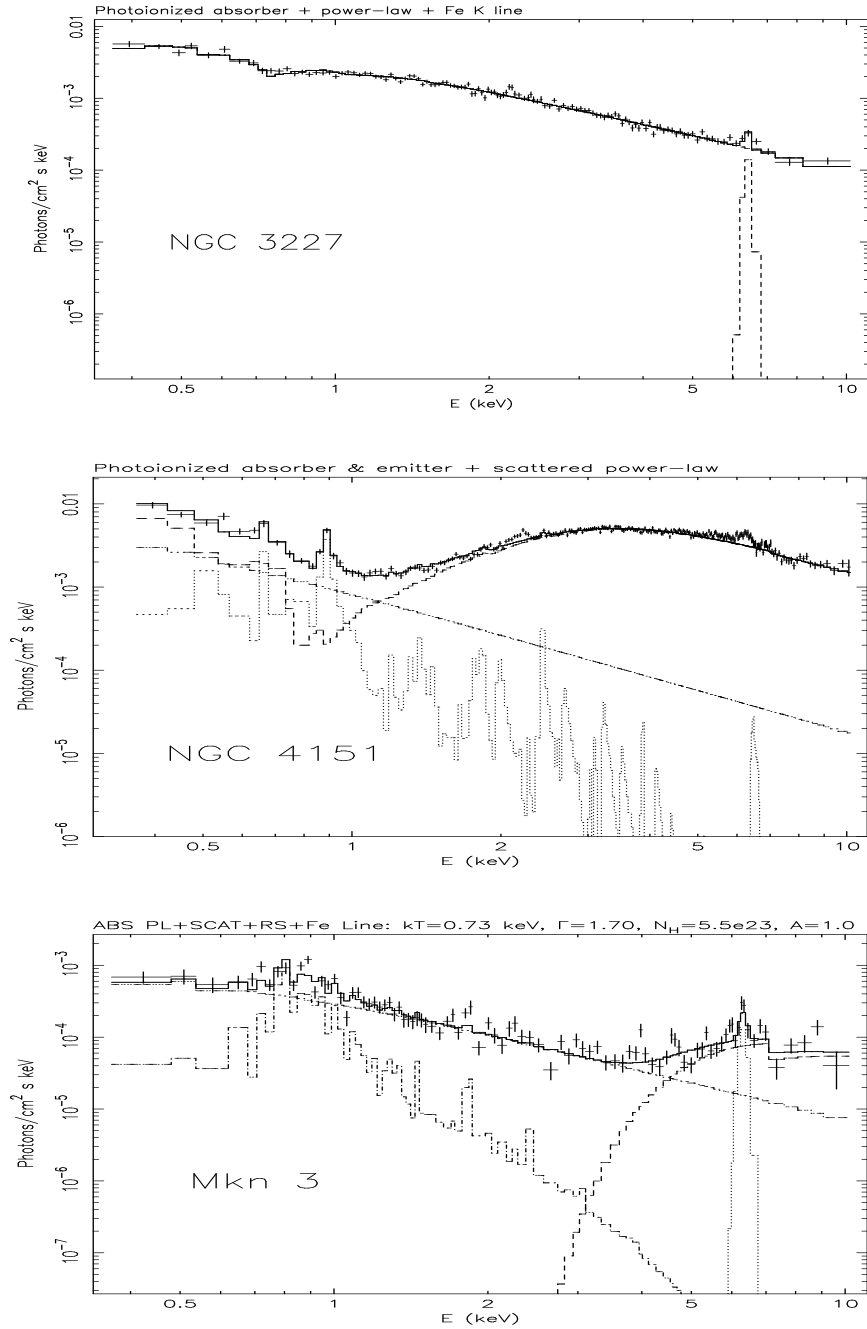


Figure 4. *ASCA* unfolded S0 spectra of a typical Seyfert 1 (NGC 3227), Seyfert 1.5 (NGC 4151) and a Seyfert 2 galaxy (Mkn 3). For details of the best-fitting models see Ptak *et al.* (1994), Weaver *et al.* (1994), and Iwasawa *et al.* (1994) for NGC 3227, NGC 4151 and Mkn 3 respectively.

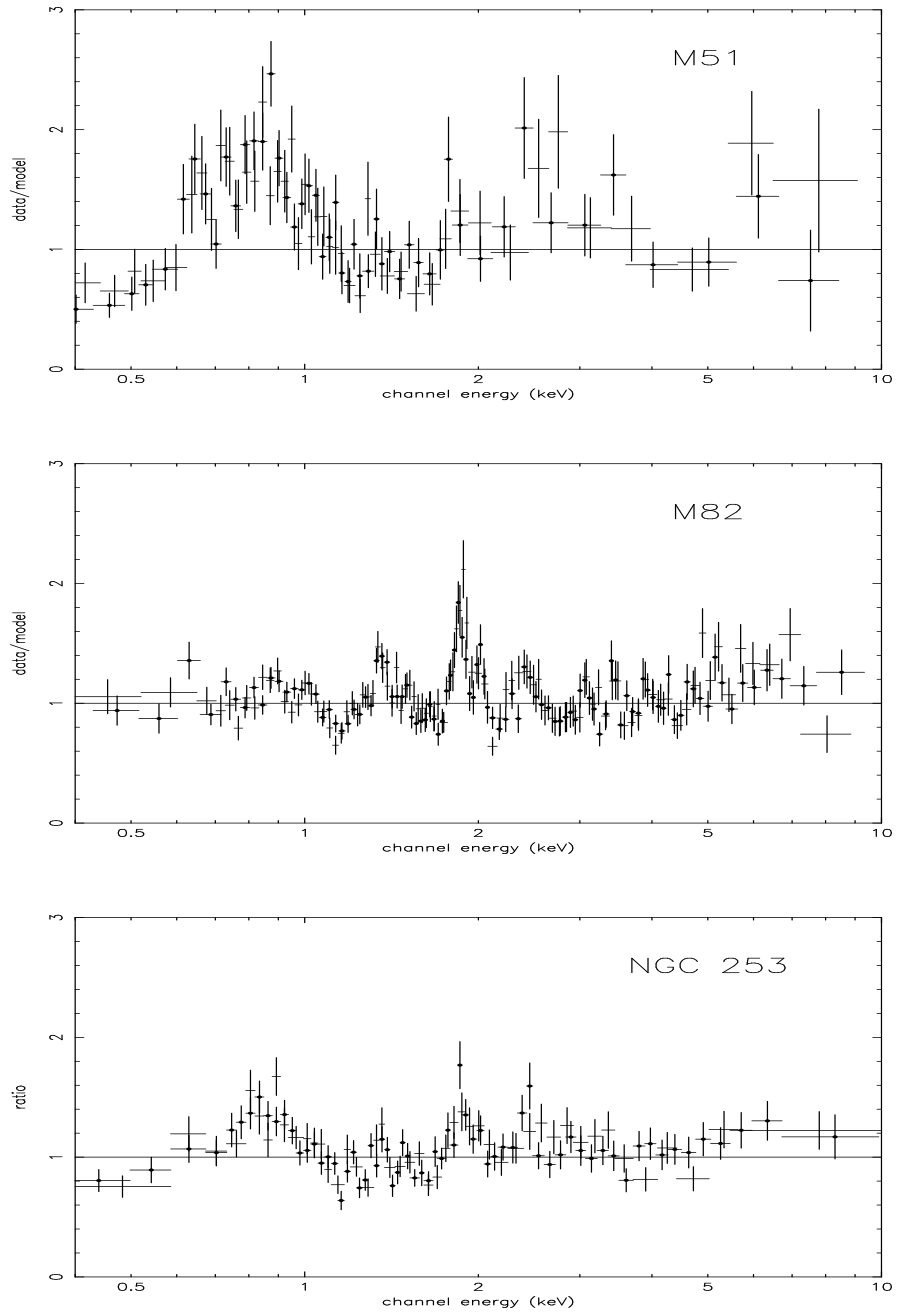


Figure 5. Residuals from fitting with an absorbed power-law + bremsstrahlung model, with line-like features clearly evident. Only data from S0 and S1 are shown for clarity, with S0 points marked with filled circles. These lines correspond to O VIII (0.65 keV), the Fe-L complex ($\sim 0.8 - 1.0$ keV), Mg XI-XII (1.35, 1.48 keV), Si XIII-XIV (1.87, 2.01 keV), and S XV (2.46 keV).

Table 3. Observed Fluxes and Luminosities

Galaxy	$F_{0.5-2.0 \text{ keV}}^{\text{PSPC}}$	$F_{0.5-2.0 \text{ keV}}^{\dagger}$	$L_{0.5-2.0 \text{ keV}}^{\ddagger}$	$L_{0.5-2.0 \text{ keV}}^{\ddagger,*}$	$F_{2-10 \text{ keV}}^{\dagger}$	$L_{2-10 \text{ keV}}^{\ddagger}$
N3998	5.0	4.0	28.	3.3	6.5	46.
N4579	5.4	1.8	28		2.9	45.
N3147	1.0	0.63	24.	1.5	1.2	45.
N4594	1.5	0.87	5.3	2.2	1.9	12.
N3310	0.67	0.72	3.2	0.76	1.3	5.9
N3079	0.48	0.44	4.4	0.4	0.53	5.3
N4258 ^a	2.0	1.2	1.5	1.5	2.9	3.6
M82	11.	7.7	1.2	0.94	18.	2.8
N3628	0.61	0.17	0.45	0.16	0.85	2.3
M81	5.8	7.7	1.2	0.28	13.6	2.1
M51	1.6	1.1	2.5	2.4	0.75	1.8
N6946	1.4	1.0	0.82	0.80	0.82	0.68
N253	3.0	2.3	0.17	0.03	4.0	0.30
N1313 ^b	1.1	0.54	0.13		1.2	0.29
M33 ^c	6.3	5.7	0.10		9.5	0.16

[†] (10^{-12} ergs s⁻¹ cm⁻²)

[‡] (10^{40} ergs s⁻¹)

* Soft component only

^a Makishima *et al.* (1994)

^b Source A in Petre *et al.* (1994)

^c Takano *et al.* (1994)

stability than the SIS). However, short-term variability in the *ROSAT* bandpass has been observed in a point source in M82 (Collura *et al.* 1994). Long-term variability, on the other hand, has been observed in many of these galaxies (several LINERs in Reichert *et al.* 1994; source B in NGC 1313 in Petre *et al.* 1994; NGC 3628 in Yaqoob *et al.* 1995a and Dahlem *et al.* 1995). Variability is also clearly evident among the *ROSAT* and *ASCA* 0.5-2.0 keV fluxes for some of the galaxies listed in Table 3.

6. The Nuclear Source in M81: A Case Study

The nearby spiral galaxy M81 is the brightest of the known LINERs and has been the subject of many detailed investigations. Extensive studies in the X-ray band have been carried out with *Einstein* (Elvis & van Speybroeck 1982; Fabbiano 1988), *GINGA* (Ohashi & Tsuru 1992), *ROSAT* (Boller *et al.* 1992) and *BBXRT* (Petre *et al.* 1993). Although at least 9 X-ray sources have been resolved using *Einstein* data, the emission is dominated by the nuclear source (also known as X-5). One of the motivating forces for studying LINERs and M81 in particular is that it has often been suggested that LINERs represent the missing link between nearby ‘normal’ galaxies and AGN. Studying the X-ray spectra of LINERs and comparison with the large body of knowledge of the X-ray properties of AGN can provide powerful diagnoses. The nuclear source in M81 has been recognized as an active nucleus for some time (Peimbert & Torres-Peimbert 1981). Prior to *ASCA* it was known that the X-ray continuum

above ~ 1 keV is likely to be due mainly to a nonthermal component (evidenced by the lack of strong soft X-ray line emission), with a photon power-law index of $\Gamma \sim 2.0 - 2.2$. Note however that *Einstein* measured a much steeper spectrum (the reason is still unknown). Long-term flux variability has been observed and even short-term variability (factor of 2 in ~ 600 s) has been reported (Mushotzky, private communication).

ASCA observed M81 on ten occasions between April 1993 and April 1995, providing the first high statistical quality, high sensitivity, moderate energy-resolution, spatially resolved hard X-ray spectra of the nuclear source. These observations also provide the first opportunity to study hard X-ray variability free from the ambiguities of non-imaging data. Here we present preliminary results using archival data combined from three of the observations which were made with the *ASCA* instruments in similar modes of operation, between April 16 and May 1 in 1993. Ishisaki *et al.* (1996) have presented results from eight of the ten observations, three of which are not yet public as of November 1995. Ishisaki *et al.* (1996) report the discovery of Fe K line emission which may have a broad and/or complex structure. However the line parameters obtained from the SIS and GIS (and indeed the continuum parameters) are discrepant and one of the goals of our independent analysis is to investigate this discrepancy. Whether there is a single complex line or multiple iron line components and whether the line(s) originate in hot or cold matter has important consequences for models of the structure of the active nucleus. A more detailed study resulting from this preliminary work will be published elsewhere.

6.1. The ASCA Data

Details of the ten *ASCA* observations of M81 can be found in Table 1 of Ishisaki *et al.* (1996). The observations were made with the SIS in different clocking modes and split thresholds. Moreover, in all four instruments, X-5 was placed on different physical positions on the detectors in different observations. However in observations 3 to 5 (as listed in Ishisaki *et al.* 1996) the SIS operation modes were the same, the source was placed in the same position on each detector and was at similar intensity levels. Thus, in order to minimize the introduction of systematic errors we use the combined data from only these three observations in order to investigate the spectral shape and the iron line emission. We combined SIS data taken in FAINT and BRIGHT modes and did *not* correct for the so-called Dark Frame Error (DFE). This may broaden the energy resolution of the SIS somewhat and may induce energy shifts of the order $\sim 10 - 30$ eV. We obtained four spectra with exposure times in the range 99–124 Ks (after cleaning).

Note that X-5 was *not* positioned on one of the nominal SIS chips in these three observations (i.e. chip 1 for S0 and chip 3 for S1). The SIS calibration is less certain for the non-standard chips since almost all of the point-source *ASCA* observations are made on the nominal chips. Individual spectra were extracted from a circle of radius 2' for the SIS and 3' for the GIS. As estimated by Ishisaki *et al.* (1996), even for a 3' circle the contamination from the nearby supernova, SN1993J, and the source X-6, should be less than 10%. Background spectra were obtained from source-free parts of the detectors (the integration

times being large enough to compensate for the small areas of the background regions).

6.2. X-ray Variability

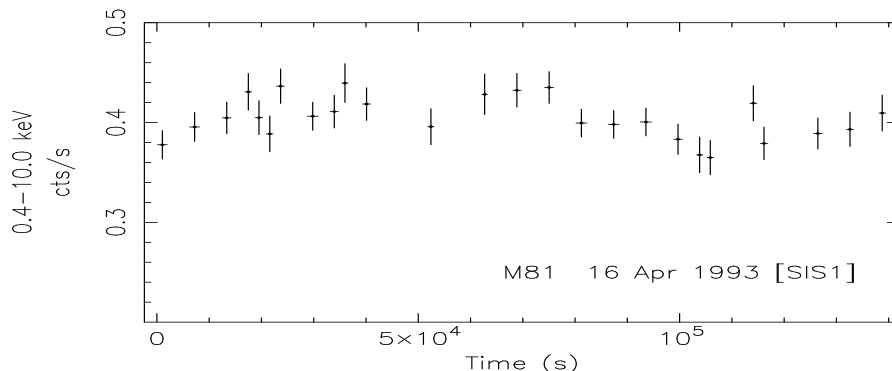


Figure 6. The S1 light curve of the extended observation of M81 during 1993, April 16–18. The data are binned at 2056 s. Note that the source is not close to the edges of the chip reducing the effects of positional instability on the light curve.

Figure 6 shows the 0.4–10 keV SIS1 light curve from the longest of the ten ASCA observations which spanned almost 2 days between April 16–18 1993. SIS1 yields the highest count-rate among the four instruments in this case. Variability of the order of $\sim 20\%$ on a timescale of hours is evident and this is typical of this source (see also Ishisaki *et al.* 1996). Among the eight observations analysed by Ishisaki *et al.* (1996), long term variability by a factor of up to ~ 1.7 was found corresponding to a 2–10 keV flux in the range $1.4\text{--}2.4 \times 10^{-11} \text{ erg cm}^{-2} \text{ s}^{-1}$ and 2–10 keV luminosity in the range $4.2\text{--}7.4 \times 10^{40} \text{ ergs}^{-1}$ ($H_0 = 50 \text{ km s}^{-1} \text{ Mpc}^{-1}$ is assumed throughout).

6.3. Spectral Fitting

Figure 7 shows the result of fitting the combined data from observations 3–5 with a simple power law plus absorber model. Due to the different properties of the SIS and GIS instruments, simultaneous fits are performed with S0 and S1 and then repeated with G2 and G3 together. A highly significant iron emission line feature is evident in both SIS and GIS data. In the SIS two line-like features are also seen at soft X-ray energies but these may be, at least in part, instrumental features. They will subsequently be modelled with simple Gaussians. The iron K feature is also first modelled with a single Gaussian. The results are shown in Table 4 and Figure 8 shows the ratio of data to best-fitting model. The photon index, Γ , is different at the 90% confidence level for the SIS and GIS. This may be due in part to the larger integration region and spatial resolution of the GIS, leading to greater contamination. Also, the GIS is not sensitive to such small column densities (Γ and N_H are correlated parameters). The SIS column is consistent with the Galactic value of $4.3 \times 10^{20} \text{ cm}^{-2}$.

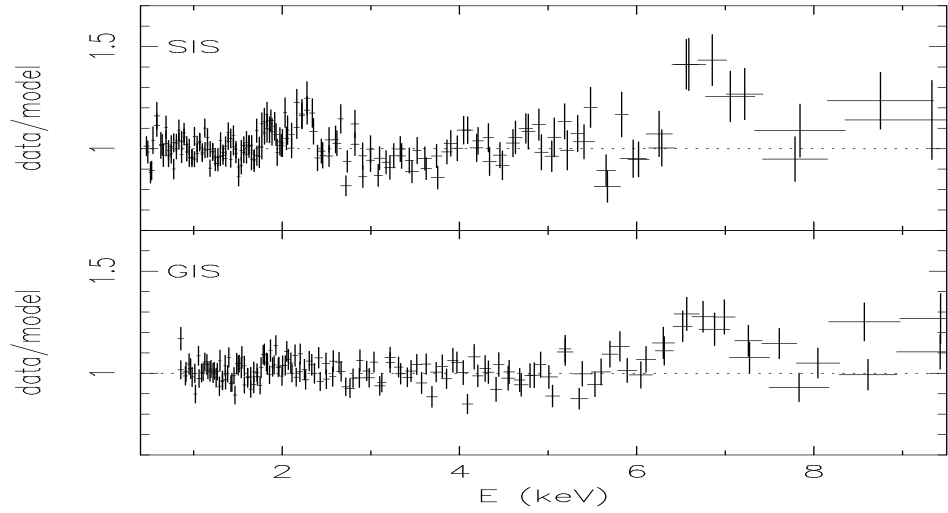


Figure 7. Ratio of M81 *ASCA* data to best-fitting power-law plus absorber model, showing the iron K line residuals.

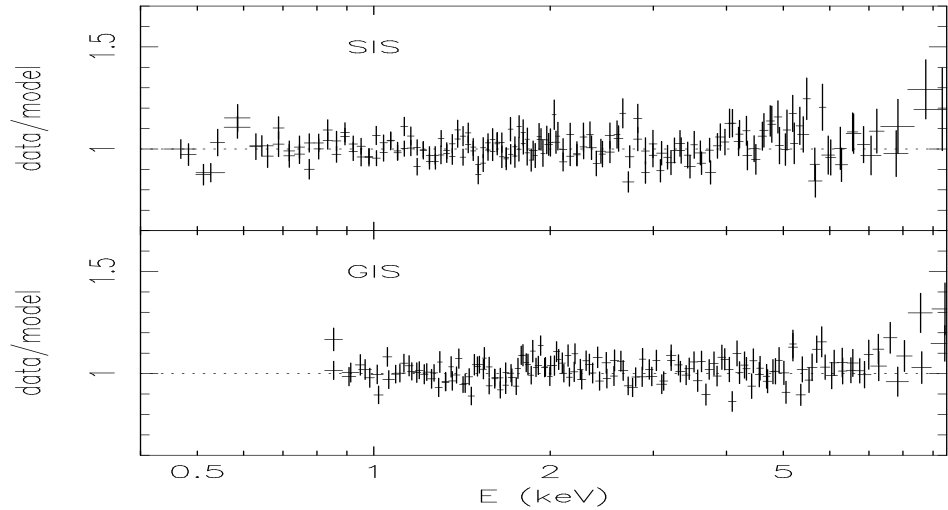


Figure 8. Ratio of M81 *ASCA* data to best-fitting power-law plus absorber model, including a single Gaussian model for the iron K line.

The SIS and GIS iron line parameters *are* consistent with each other. See Table 4 and Figure 9 which shows confidence contours of the line energy (E_{Fe}) and intrinsic Gaussian width (σ_{Fe}). The line is required to be broader than the SIS resolution at a high level of confidence. The best-fitting SIS width corresponds to ~ 0.71 keV FWHM or $\sim 30,000$ km s $^{-1}$ FWHM. The line energy is consistent with an origin in He-like iron. The equivalent width (EW) of the line is large, $\sim 200 - 400$ eV and may be problematic for models of the line emission (see §6.4).

Table 4. Power Law Plus Absorber and Single Gaussian Model

DET	Γ	N_H (10^{20} cm^{-2})	E_{Fe} (keV)	σ_{Fe} (keV)	I_{Fe}^a	EW (eV)	χ^2 (dof)
S0,S1	$1.91^{+0.04}_{-0.05}$	$6.5^{+0.13}_{-0.13}$	$6.78^{+0.24}_{-0.22}$	$0.30^{+0.26}_{-0.17}$	$4.2^{+2.5}_{-2.3}$	385^{+229}_{-211}	476.5 (412)
S2,S3	$1.72^{+0.05}_{-0.03}$	$0.0^{+4.4}_{-0.0}$	$6.68^{+0.19}_{-0.18}$	$0.21^{+0.34}_{-0.21}$	$3.0^{+2.1}_{-1.6}$	228^{+160}_{-122}	1023 (970)

Errors are 90% confidence for 5 interesting parameters.
^a Iron line intensity in units of $10^{-5} \text{ photons cm}^{-2} \text{ s}^{-1}$.

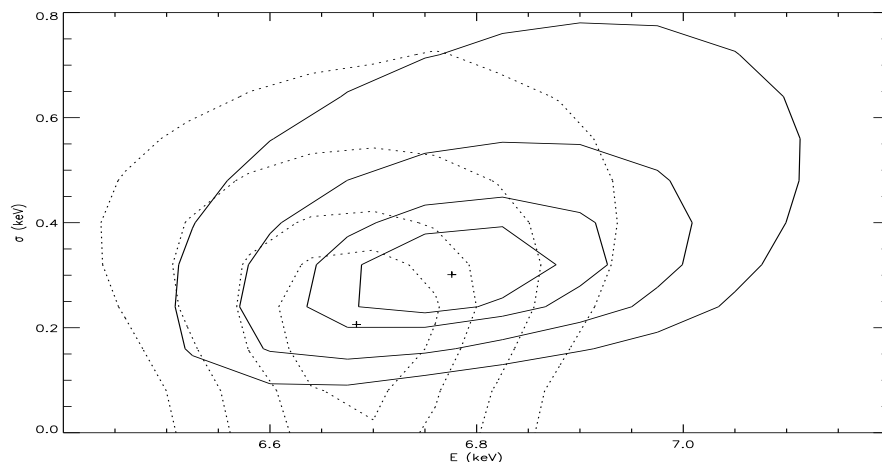


Figure 9. Confidence contours of the center energy and intrinsic width of the iron K line in M81 when it is modelled with a single Gaussian. The contour levels for the SIS data (solid lines) and the GIS data (dotted lines) correspond to 68%, 90% and 99% for 2 interesting parameters and the final contour to 99% for 5 interesting parameters ($\Delta\chi^2 = 2.279, 4.605, 9.21$ and 15.086 respectively). Note that the third contour is approximately equal to 90% confidence for 5 interesting parameters ($\Delta\chi^2 = 9.24$).

The 0.5–2 keV and 2–10 keV fluxes averaged over four instruments are 7.7 and $13.6 \times 10^{-12} \text{ erg cm}^{-2} \text{ s}^{-1}$ respectively, corresponding to luminosities of 2.4 and $4.2 \times 10^{40} \text{ erg s}^{-1}$ respectively. In order to test for the presence of an additional soft component we added a Raymond-Smith component and obtained a reduction in χ^2 of 14 (SIS) and 3 (GIS) for four additional parameters (two normalizations, temperature and metal abundance). For the SIS we obtained $KT \sim 1.25 \text{ keV}$ and negligible metal abundance (< 0.01 relative to cosmic).

Thus, the case for an additional soft continuum component is not strong. Note that thermal models of the *hard* continuum are very strongly ruled out.

6.4. Origin of the Iron K Emission

In order to investigate the origin of the iron K line we performed additional spectral fits using the SIS data as follows.

1. Multiple Line Complex To test the possibility that a multiple set of narrow lines may be mimicking a a broad line, we replaced the single broad Gaussian in §6.3 with three narrow Gaussians (intrinsic width of each fixed at 0.1 keV). The best-fitting energies are 6.52, 6.76, and 7.15 keV with corresponding equivalent widths of 95, 65 and 178 eV respectively. We get $\chi^2 = 499.8$ (409 d.o.f.) which, even with three more free parameters, is higher by 23.3 than the χ^2 for the single broad Gaussian model. If the intrinsic widths of the lines are allowed to be free, two of the lines are forced to zero intensity and the single broad Gaussian solution is once again recovered.

2. Thermal Comptonization We replaced the single broad Gaussian in §6.3 with a model of a monochromatic line broadened by Compton scattering in plasma with temperature kT and optical depth τ (both free parameters). The best-fitting values are $kT = 13.1$ keV and $\tau = 0.15$ but $\chi^2 = 508$ (412 d.o.f.) which is 31.5 higher than the single broad Gaussian model, yet the number of free parameters is the same in each case.

3. Relativistic Disk Model We also tried a relativistic disk model for the iron line profile. See, for example Tanaka *et al.* (1995) and Yaqoob *et al.* (1995b) where the model has been applied to the iron line profiles in the Seyfert galaxies MCG -6-30-15 and NGC 4151 respectively. The best-fitting rest-frame line energy is 6.73 keV but the 90% confidence errors allow any value in the range 6.4–6.9 keV so it was fixed at its best-fitting value. We obtained $\chi^2 = 480$ (412 d.o.f.) and a disk inclination angle of 40_{-12}^{+10} degrees and an EW of 523 ± 245 eV. It is difficult to produce such a large equivalent width without increasing the iron abundance significantly above solar. The same problem has been encountered with the broad lines detected in some classical Seyfert 1 and 2 galaxies (see discussions in Mushotzky *et al.* 1995; Tanaka *et al.* 1995; Fabian *et al.* 1995; Yaqoob *et al.* 1995b). However, if the line rest-frame energy is really ~ 6.7 keV or higher then an ionized disk would account for the large equivalent width (e.g. Matt *et al.* 1993). A possible problem with this interpretation is the low accretion rate compared to Eddington. Note that the data can accommodate the reflected continuum from such a disk but cannot constrain it.

6.5. Conclusions

The X-ray continuum of M81 appears to have a nonthermal, power-law form and we find little evidence of any additional, soft X-ray continuum. Some of the X-ray properties of the AGN in M81 are similar to classical Seyfert 1 galaxies whilst others have more in common with higher luminosity AGN, or quasars. The properties of the broad iron line in M81 are similar to those recently found by *ASCA* for several Seyfert 1 galaxies. The broadening mechanism, namely Doppler and/or gravitational redshifts in matter close to the X-ray source may also be similar in M81 and Seyfert 1s. If the matter is in the form of a disk then the inclination angle relative to the observer is ~ 40 degrees. The photon index

($\Gamma \sim 1.9$) of the power-law continuum is similar to that observed in quasars and is also similar to that thought to be the *intrinsic* photon index in Seyfert 1s (e.g. Nandra & Pounds 1994). Thus the origin of the hard X-ray continuum *may be the same* in LINERS, Seyfert galaxies and quasars, with the caveat that in Seyfert 1s the *observed* continuum has been reprocessed by matter out of the line-of-sight and in Seyfert 2s the observed continuum is most affected by line-of-sight reprocessing.

AGN with X-ray luminosities of the order $\sim 10^{41} - 10^{42}$ erg s $^{-1}$ typically vary rapidly by factors $\sim 2 - 3$ on a timescale of hours or less, whilst higher luminosity AGN are more sluggish. On other hand, rapid variability is not typical of the AGN in M81. This is puzzling, suggesting that rapid variability only occurs for a restricted range in AGN luminosities, covering 2-3 decades.

7. Discussion

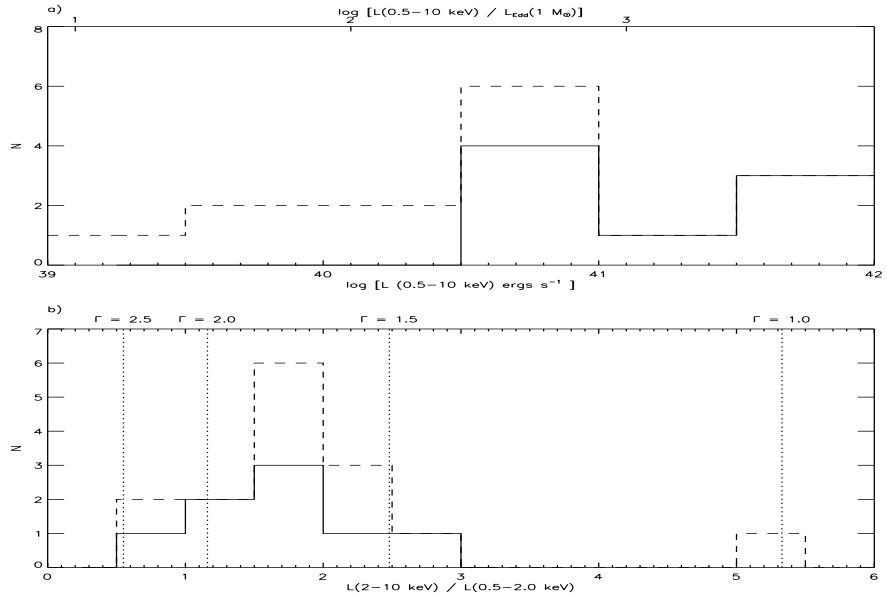


Figure 10. **a)** 0.5-10 keV luminosities of the galaxy sample. Solid line shows LINERs/LLAGN only. Top axis shows log of number of solar-mass binaries emitting at the Eddington luminosity required to produce the luminosities shown. **b)** As in a) but with hardness ratios. The dotted lines show the expected hardness ratio from an absorbed power-laws with photon indices of 2.5, 2.0, 1.5 and 1.0

The hard X-ray emission of both starburst and LINER galaxies is usually dominated by a compact nuclear, or near-nuclear source and there are often one to several other off-nuclear X-ray sources in the galaxy which together constitute the bulk of the X-ray luminosity. Figure 10a shows a histogram of the luminosities observed in the entire galaxy sample, with LINERs/LLAGN (NGC 3147, NGC 3998, NGC 4579, NGC 4594, NGC 4258, M51, NGC 3079, M81) plotted

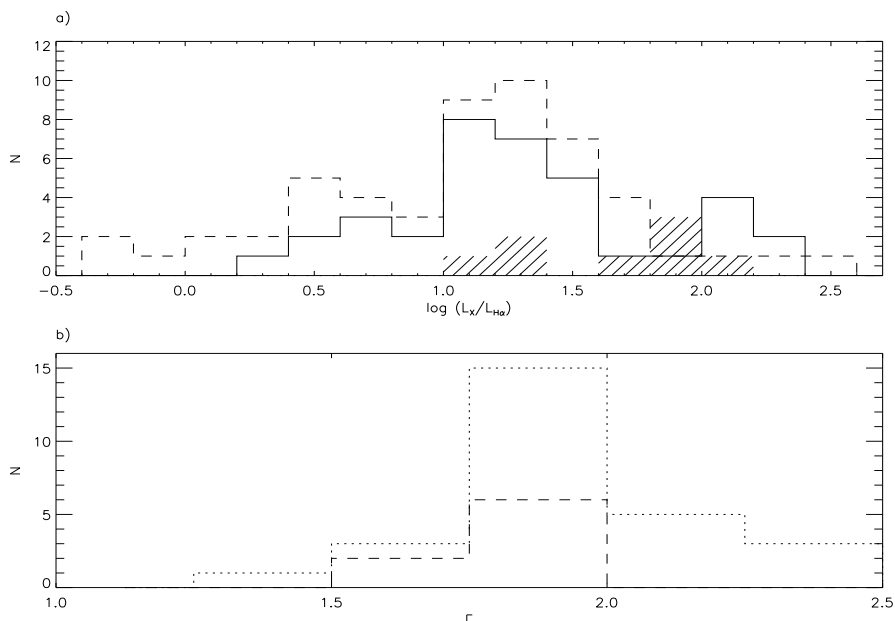


Figure 11. **a)** Distribution of $L_X/L_{H\alpha}$ for AGN observed in the 0.5-4.5 keV band (dashed line) and 2-10 keV band (solid line) from Elvis, Soltan, & Keel (1984), with the filled bars showing the *ASCA* results in the 2-10 keV band for 8 LINERs/LLAGN. **b)** Distribution of photon indices (Γ) observed in the power-law component of LINERs/LLAGNs (dashed line) and the Nandra & Pounds (1994) sample of Seyfert 1 AGN (dotted line) (the Nandra & Pounds (1994) slopes are from fits including Compton reflection)

separately. LINER/LLAGN are more luminous than the starburst galaxies, in general. In both cases, tens to thousands of solar-mass X-ray binaries radiating at the Eddington limit would be required to produce the observed flux. Also shown (Figure 10b) is a histogram of the hardness ratio (2-10 keV flux / 0.5-2.0 keV flux) from which it can be seen that there is no clear separation between the starbursts and the LINER/LLAGN. Most of the galaxies have a hardness ratio similar that expected from an unabsorbed power-law with $\Gamma \sim 1.5 - 2.5$. An exception is NGC 3628 (traditionally classified as a starburst) which has an exceptionally flat X-ray spectrum with $\Gamma \sim 1.2$ (Yaqoob *et al.* 1995a).

Variability has been observed in both LINER and starburst galaxies on timescales of weeks to years. This implies that in both starbursts and LINERs, a significant amount of the emission is originating from a compact ($\ll 1$ pc) region, most likely due to a single object such as a LLAGN or X-ray binary (although such a binary would have to have a much larger mass than known X-ray binaries, typically $\sim 10 - 1000 M_{\odot}$). On the other hand, rapid variability, on timescales of a day or less, is *not* observed. Thus, if LLAGN are simply low-luminosity versions of classical AGN, it is puzzling that rapid variability is most common in objects with 2-10 keV luminosity in the range $\sim 10^{42} - 10^{43}$ erg s $^{-1}$ but vanishes below $\sim 10^{41}$ erg s $^{-1}$.

These results strongly imply a connection between starburst and LINER activity, with the soft component most likely being produced by warm gas with $kT \sim 0.6 - 0.8$ keV, possibly from an SNR-heated ISM and starburst-driven

winds. In some cases, the hard component of both starburst and LINERs may also be due to starburst activity, possibly resulting from compact supernovae (cSNR). It is possible that some LINERs (and starbursts) may be powered by AGN-type accretion. To test this hypothesis we have plotted histograms of the ratio of X-ray flux to H_α flux and the photon indices (Γ) observed in the LINERs/AGN along with the same quantities for AGN in Figures 11a and 11b, respectively. There is no obvious distinction between the two groups. Unfortunately, our sample is too small to statistically test if the two samples originated from the same parent population, however, Figures 11a and 11b suggest that this is the case.

The X-ray spectra of LINERs and starbursts are not very different to those of classical AGN. The hard power-law slopes are similar to those of quasars and the inferred *intrinsic* slopes of Seyfert galaxies. It appears that quasars and the low-luminosity spiral galaxies are devoid of large amounts of matter residing in the nucleus, which is responsible for reprocessing the X-ray continua of the intermediate luminosity Seyfert galaxies (e.g. Nandra & Pounds 1994). Even the soft extended thermal emission which is common in many of the LINERs and starbursts has been observed in classical AGN in which the hard power-law is heavily absorbed, allowing the soft component to be detected (e.g. NGC 4151 and Mkn 3; see Figure 4).

Another puzzling result is the lack of significant Fe-K line emission in galaxies like NGC 253 and M82 which are thought to be prototypical starburst galaxies in which case the hard X-ray emission would be expected to have a thermal origin. Yet, the lack of Fe-K line emission and the OSSE detection of NGC 253 (Bhattacharya *et al.* 1994) suggest a nonthermal origin. Fe-K line emission (in all cases, likely to be due to fluorescence) is clearly detected in only three of the galaxies: NGC 3147 (Ptak *et al.* 1996), NGC 4258 (Makishima *et al.* 1994) and M81 (Ishisaki *et al.* 1996 and §6). In the first two cases the Fe-K line very likely originates in obscuring matter around the nucleus, in close analogy to the mechanism in Seyfert 2 galaxies. In the case of M81 the characteristics of the Fe-K line are very similar to those in Seyfert 1 galaxies and the line may indeed have the same origin; an X-ray illuminated accretion disk. The inferred low accretion rate of M81 may however be problematic. Much work remains to be done in understanding the physical implications of the X-ray emission in low-luminosity spiral galaxies.

Acknowledgments. We thank Rich Mushotzky and Hagai Netzer for useful discussions. We also would like to thank Gail Reichert for sharing her results prior to publication. This research has made use of data obtained through the High Energy Astrophysics Science Archive Research Center Online Service, provided by the NASA-Goddard Space Flight Center and the NASA/IPAC Extragalactic Database (NED) which is operated by the Jet Propulsion Laboratory, Caltech, under contract with NASA.

References

- Bhattacharya, D., *et al.* 1994, ApJ, 437, 173
 Boller, *et al.* 1992, A&A, 261, 57

Collura, A., Reale, F., Schulman, E., & Bregman, J. 1994, ApJ, 420, L63
 Dahlem, M., Heckman, T. & Fabbiano, G. 1995, ApJ, 442, L49
 Elvis, M. & Speybroeck, L. 1982, ApJ, 257, L51
 Elvis, M., Soltan, A., & Keel, W. 1984, ApJ, 283, 479
 Fabbiano, G. & Trinchieri, G. 1984, ApJ, 268, 491
 Fabbiano, G. 1988, ApJ, 325, 544
 Fabian, A., *et al.* 1995, MNRAS, 277, L11
 Heckman, T. 1980, A&A, 88, 365
 Ishisaki, Y., *et al.* 1996, in press
 Iwasawa, K., Yaqoob, T., Awaki, H. & Ogasaka, Y., 1994, PASJ, 46, L167
 Makishima, K., *et al.* 1994, PASJ, 46, L77
 Marston, A., Elmegreen, D., Elmegreen, B., Forman, W., Jones, C., & Flanagan, K. 1995, ApJ, 438, 663
 Matt, G., Fabian, A. C., & Ross, R. R. 1993, MNRAS, 262, 179
 Mushotzky, R., *et al.* 1995, MNRAS, 272, L9
 Nandra, K. & Pounds K. 1994, MNRAS, 268, 405
 Ohashi, T. & Tsuru, T. 1992 in *Frontiers in X-ray Astronomy*, eds. Y. Tanaka and K. Koyoma, 435
 Petre, R. 1993, in *The Nearest Active Galaxies*, eds. J. Beckman, L. Colina, and H. Netzer, 117
 Petre, R., *et al.* 1993, ApJ, 418, 644
 Petre, *et al.* 1994, PASJ, 46, L115
 Peimbert M. & Torres-Peimbert S. 1981, ApJ, 245, 845
 Ptak, A., Yaqoob, Y., Serlemitsos, P., Mushotzky, R., & Otani, C. 1994, ApJ, 436, L31
 Ptak, A., Yaqoob, T., Serlemitsos, P., J., Kunieda, H., & Terashima, Y. 1996, ApJ, Mar 10 issue
 Reichert, G., Mushotzky, R., & Filippenko, A. 1994, in *The Soft X-ray Cosmos*, eds. E. Schlegel and R. Petre, 85
 Takano, M., Mitsuda, K., Fukazawa, Y., & Nagase, F. 1994, ApJ, 436, L41
 Tanaka, Y., Inoue, H., & Holt, S. 1994, PASJ, 46, L37
 Tanaka, Y., *et al.* 1995, Nature, 375, 659
 Terashima, Y., *et al.* 1994, in *New Horizon of X-ray Astronomy*, eds. F. Makino and T. Ohashi, 523
 Terashima, Y., *et al.* 1996, in preparation
 Tsuru, T., *et al.* 1994, in *New Horizon of X-ray Astronomy*, eds. F. Makino and T. Ohashi, 529
 Weaver, K., Yaqoob, T., Holt, S., Mushotzky, R., Matsuoka, M., & Yamauchi, M. 1994, 436, L27
 Yaqoob, T., Serlemitsos, P., Ptak, A., Mushotzky, R., Kunieda, H., & Terashima, Y. 1995a, ApJ, Dec 20 issue
 Yaqoob, T., *et al.* 1995b, ApJ, 453, L81